

PTB-TIR: A Thermal Infrared Pedestrian Tracking Benchmark

Qiao Liu, *Student Member, IEEE*, Zhenyu He, *Senior Member, IEEE*,

Abstract—Thermal infrared (TIR) pedestrian tracking is one of the most important components in numerous applications of computer vision, which has a major advantage: it can track the pedestrians in total darkness. How to evaluate the TIR pedestrian tracker fairly on a benchmark dataset is significant for the development of this field. However, there is no a benchmark dataset. In this paper, we develop a TIR pedestrian tracking dataset for the TIR pedestrian tracker evaluation. The dataset includes 60 thermal sequences with manual annotations. Each sequence has nine attribute labels for the attribute based evaluation. In addition to the dataset, we carry out the large-scale evaluation experiments on our benchmark dataset using nine public available trackers. The experimental results help us to understand the strength and weakness of these trackers. What’s more, in order to get insight into the TIR pedestrian tracker more sufficiently, we divide a tracker into three components: feature extractor, motion model, and observation model. Then, we conduct three comparison experiments on our benchmark dataset to validate how each component affects the tracker’s performance. The findings of these experiments provide some guidelines for future research.

Index Terms—thermal infrared, pedestrian tracking, benchmark, dataset

I. INTRODUCTION

Along with the development of thermal imaging technology, both quality and resolution of the thermal images have been improved to a great extent. That enables a series of computer vision tasks based on thermal images can be applied to the civilian field. TIR pedestrian tracking is one of the most important vision tasks which has received much attention in recent years. It has wide applications such as surveillance, driving assistance, and rescue at night [1]. Numerous TIR pedestrian trackers [2]–[8] have been proposed over the past decade. Despite much progress has been achieved, TIR pedestrian tracking still faces many challenges, e.g., occlusion, background clutter, motion blur, low resolution, thermal crossover, etc.

Evaluating and comparing the TIR pedestrian tracker fairly is crucial for the development of this field. Usually, there is not a single tracker that can handle all challenges. Therefore, it is necessary to compare and analyze the strength and weakness of each tracker, thereby giving some guidelines to the future study for a better tracker. In order to do that, it is critical to collect a representative dataset. Several TIR datasets are used, such as OSU Color-Thermal [9], Terravic Motion IR [10], PDT-ATV [11], and BU-TIV [12] databases. However, it can

not fair compare the TIR pedestrian tracker on these datasets due to the following reasons. First, these datasets just have a few sequences that are not sufficient for fair evaluation. Second, the thermal images just are captured from a thermal camera that lacks diversity. Third, the thermal images have low resolution and static background that not suit to various real-world scenarios. Fourth, these datasets do not provide a unified ground-truth and attribute annotations. All of these reasons show that this field lacks a benchmark dataset to fair evaluate the TIR pedestrian tracker.

Modern TIR pedestrian tracker is a complicated system which is consisted of several separate components. Each component can affect its performance. Evaluating a TIR pedestrian tracker as a whole helps us to understand its overall performance, but cannot know the effectiveness of each component. To understand the TIR pedestrian tracker more sufficiently, it is necessary to compare each component separately. Similar to [13], we divide the TIR pedestrian tracker into three components: feature extractor, motion model, and observation model. After dividing, some interesting questions will be raised involuntarily. Which feature is more suitable for TIR pedestrian tracking? How different motion models and observation models affect the tracking performance? The answers to these questions provide some references to the direction of future research.

In this paper, to fair evaluate and compare TIR pedestrian trackers, we first collect a TIR pedestrian dataset¹ for short-term tracking task. The dataset includes 60 video sequences with manual annotations. The entire dataset is divided into nine different attribute subsets. On each subset, we can evaluate the tracker’s ability of handling the corresponding challenge. Then, we carry out a large-scale fair performance evaluation on several public available trackers. Finally, in order to get insight into the TIR pedestrian tracking, we further conduct three validation experiments on three components of the tracker. First, we compare several different features on a baseline tracker to analyze which feature is more suitable for TIR pedestrian tracking. Second, we compare several different motion models on a baseline tracker to analyze how they affect the tracking results. Third, to explore how different observation models affect the tracking performance, we compare several trackers with different observation models. The findings of these three experiments make us understand the TIR pedestrian tracker more sufficiently.

The contributions of the paper are two-fold:

Q. Liu, Z. He (Corresponding author) are with the School of Computer Science and Technology, Harbin Institute of Technology, Shenzhen, China. e-mail: (zhenyuhe@hit.edu.cn).

¹The PTB-TIR dataset and code library can be accessed at <http://www.hezhenyu.cn/PTB-TIR.html>

TABLE I: Comparison of our dataset with other datasets.

	OSU Color-Thermal [9]	Terravic Motion IR [10]	PDT-ATV [11]	BU-TIV [12]	PTB-TIR (Ours)
Device Type	Raytheon PalmIR 250D	Raytheon Thermal-Eye 2000AS	FLIR Tau 320	FLIR SC8000	More than 8 sources
Resolution	320×240	320×240	324×256	up to 1024×640	up to 1280×720
Bit Depth	8	8	8	16	8
Sequences Number	3	11	8	5	60
Mean Length	2848	500	486	4530	502
Total Frames	8544	5500	3888	22654	30128

- We construct a TIR pedestrian tracking benchmark dataset with 60 annotated sequences for the TIR pedestrian tracker evaluation. A large-scale performance evaluation is implemented on our benchmark with several public available trackers.
- Several validation experiments on the proposed benchmark are carried out to get insight into the TIR pedestrian tracking system. The experimental findings are analyzed to given some guidelines for future research.

The rest of the paper is organized as follows. We first introduce TIR pedestrian tracking datasets and methods briefly in Section II. Then, we present the contents of the proposed benchmark in Section III. Subsequently, the extensive performance evaluation and validation experiments are carried out in Section IV and Section V respectively. Finally, we draw a short conclusion and describe some future works in Section VI.

II. RELATED WORK

In this section, we first introduce existing datasets which can be used for TIR pedestrian tracking in Section II-A. Then, we discuss the progress of the TIR pedestrian tracking methods in Section II-B.

A. TIR Pedestrian Tracking Datasets

There is no a standard and specialized TIR pedestrian tracking dataset but several datasets can be used to simply test TIR pedestrian tracker.

OSU Color-Thermal. The original purpose of this dataset [9] is to do object detection using RGB video and thermal video. The dataset contains 3 TIR pedestrian videos are captured from a fixed thermal sensor: Raytheon PalmIR 250D. These videos have a low resolution 320×240 and their backgrounds are static.

Terravic Motion IR. This dataset [10] is designed for detection and tracking task in the thermal video. It has 18 TIR sequences captured from a thermal camera Raytheon L-3 Thermal-Eye 2000AS. Among these sequences, 11 pedestrian sequences are suitable for tracking task. These sequences are all in the same wild scene with a static background and a low resolution 320×240 .

PDT-ATV. PDT-ATV [11] is a TIR pedestrian tracking and detection dataset is captured from a simulative unmanned aerial vehicle (UAV). The dataset contains 8 sequences with the same resolution 324×256 . The dataset provides manually

ground-truths of the object but not annotates the attributes of each sequence.

BU-TIV. BU-TIV [12] is a large-scale dataset for several visual analysis tasks in TIR videos. It contains 5 TIR pedestrian videos that can be used for tracking task. The resolution of these videos is ranging from 512×512 to 1024×640 . The dataset provides the annotations of the object but not offers any evaluation codes for tracking task.

Table I compares the above-mentioned datasets with our dataset. Although these datasets can be used in the TIR pedestrian tracking to test a tracker, they are not suitable for fair comparison and evaluation. In this paper, in order to fair compare and evaluate a tracker, we collect a large-scale TIR pedestrian tracking benchmark dataset with 60 annotated sequences.

B. TIR Pedestrian Tracking Methods

In the past decade, numerous TIR pedestrian tracking methods have been proposed to solve the various challenges. General speaking, there are two categories of TIR pedestrian trackers: generative and discriminative. Generative TIR pedestrian trackers focus on the modeling of pedestrian’s appearance and search the most similar candidates in the next frame. Some representative methods are template matching [14], [15], sparse representation [5], [16]. Unlike the generative methods, discriminative TIR pedestrian tracking methods cast the tracking problem as a binary classification problem which distinguishes the object target from its backgrounds. Thanks the advances of the machine learning, a series of classifier can be used in the TIR pedestrian tracking, such as random forest [4], mean shift [17], support vector machine (SVM) [18]. Here, we discuss these methods according to three components : feature extractor, motion model, and observation model.

Feature Extractor. Obtaining a powerful representation of the object target is a crucial step in TIR pedestrian tracking. Different from the visual pedestrian tracking that often uses the color feature, intensity feature is widely used in the TIR pedestrian tracking due to a basic assumption that the object target is warmer than its background in the thermal images. However, a tracker only using the intensity feature often fails when two similar pedestrians are crossing each other. In order to get more discriminative feature representation, several TIR pedestrian trackers exploit multiple features fusion strategy. For example, Wang et al. [19] combine the intensity and edge cues via an adaptive multi-cue integration scheme.



Fig. 1: Some annotated sequences of our proposed dataset. The target’s ground-truth bounding box in the first frame is shown. The sequences are ranked according to its difficult degree which is the average TRE score of the tested trackers on each sequence (see the *supplemental material*). The sequence name, difficult degree, and corresponding attributes are shown below the image respectively. **Blue** font denotes old sequences used in the previous studies, while **red** font denotes for newly collected sequences.

In [3], the authors also fuse the intensity and edge information using a relative discriminative coefficient. In [4], the authors coalesce local intensity distribution (LID) and oriented center symmetric local binary patterns (OCS-LBP) to represent the TIR pedestrian. What’s more, some other features are often used in TIR pedestrian tracking, such as regions of interest (ROI) histogram [2], speeded up robust features (SURF) [15], and the histogram of oriented gradient (HOG) [20].

Motion Model. How to quickly and accurately generate a series of target candidates in the next frame is another important component in the TIR pedestrian tracking. Usually, two kinds of methods are used to generate the target candidates: probabilistic estimation and exhaustive search. For the probabilistic estimation methods, Kalman filter and particle

filter are often exploited in TIR pedestrian tracking. For instance, Xu et al. [17] combine the Kalman filter and mean shift to track the pedestrian by a vehicle-mounted thermal camera. Wang et al. [19] propose a multiple features fusion TIR pedestrian tracker based on the particle filter framework. Several other TIR pedestrian tracking methods [2]–[4] also use the particle filter. For the exhaustive search method, there are two kinds of method are often used in visual tracking: sliding window [13] and radius sliding window [21], they also suit for TIR pedestrian tracking.

Observation Model. In the discriminative TIR pedestrian tracking methods, the observation models are used to obtain the tracked target from a series of candidates. Usually, we train a binary classifier to complete this task. Thanks to the

developments of machine learning, numerous classification methods are used. For example, Xu et al. [17] use mean shift to get the final tracked target from a series of target candidates generated from Kalman filter. Ko et al. [4] exploit random forest to obtain the tracked target from the candidates. Some other classification method, such as SVM [18], boosting [22], multiple instance learning (MIL) [23], are also suitable for TIR pedestrian tracking

These three components of the TIR pedestrian tracker affect the tracking performance in different ways. How each component affects the final tracking results? In this paper, we conduct several validation experiments on our proposed benchmark to answer this question.

III. TIR PEDESTRIAN TRACKING BENCHMARK

In this section, we first introduce our TIR pedestrian tracking dataset in Section III-A, and then, present the evaluation methodology for the TIR pedestrian tracker in Section III-B. These two parts constitute our TIR pedestrian tracking benchmark.

A. Dataset

In the past decade, several datasets [9]–[12] are used to evaluate the TIR pedestrian tracker. However, these datasets do not provide uniform ground-truths for fair evaluation. To implement fair performance evaluation and comparison for the TIR pedestrian tracker, we collect 60 thermal sequences, and then annotate them manually. These sequences come from the different devices, scenes, and shooting time. For each shooting property, we collect a series of corresponding thermal videos. More basic properties can be found in Table II. These different properties ensure the diversity of the dataset.

TABLE II: Basic properties of the shooting videos and the corresponding video number.

Property Name	Property value: video number
Device Categories	Surveillance camera: 29; Hand-held camera: 20; Vehicle-mounted camera: 8; Drone camera: 3
Scene Types	Outdoor: 52; Indoor: 8
Shooting Time	Night: 42; Day: 18
Camera Motion	Static: 43; Dynamic: 17
Camera Views	Down: 31; Level: 29
Object Distance	Far: 21; Middle: 23; Near: 16
Object Size	Big: 12; Middle: 34; Small: 14

Sources. Our datasets are collected from the existing commonly used thermal sequences and Internet. Four thermal sequences are obtained from OSU Color-Thermal dataset [9]. Six sequences are adopted from Terravic Motion IR [10] and nine sequences are chosen from BU-TIV [12]. Two sequences came from LITIV2012 [24] and five sequences came from detection dataset CVC-09 [25] and CVC-14 [26]. In addition, we select seven pedestrian videos from the TIR object tracking benchmark: VOT-TIR2016 [27]. The rest of the sequences are collected from the Internet, such as INO dataset [28] and YouTube [29].

Annotations. We use an external rectangle bounding box of the target as its ground-truth. The first frame annotations of several sequences are shown in Fig. 1. The left corner point, width, and height of the target’s bounding box are recorded to represent the ground-truth.

Attributes of a Sequence. Evaluating a TIR pedestrian tracker is usually difficult because several attributes can affect its performance. In order to better evaluate the strength and weakness of a TIR pedestrian tracker, we summarize nine common attributes in the sequences, as shown in Table III. For each attribute, we construct a corresponding subset for evaluation. The performance of a tracker on an attribute subset shows its ability for handling the corresponding challenge. The attributes distribution of the entire dataset and an attribute subset are shown in Fig. 2. The other subset’s attributes distribution are shown in the **supplemental material**. We can see that the background clutter has a high ratio because the pedestrians often have similar texture and intensity in the thermal images. In addition, the occlusion and scale variation also often occurs in the real-world scenarios. The intensity variation subset only includes three sequences due to the pedestrians tend to have invariable temperature in a short time.

TABLE III: Attributes of a thermal sequence.

Chall	Description
OCC	Occlusion: the target is partially or fully occluded.
SV	Scale variation: the ratios of the target’s size in the first frame and current frame is out of the range $[1/2, 2]$.
BC	Background clutter: the background near the target has similar texture or intensity.
LR	Low resolution: the target’s size is lower than 600 pixels.
FM	Fast motion: the distances of target in the consecutive frame are larger than 20 pixels.
MB	Motion blur: the target region is blurred due to the target or camera motion.
OV	Out-of-view: the target is partially out of the image region.
IV	Intensity variation: the intensity of the target region has changed due to the temperature variation of the target.
TC	Thermal crossover: Two targets with similar intensity cross each other.

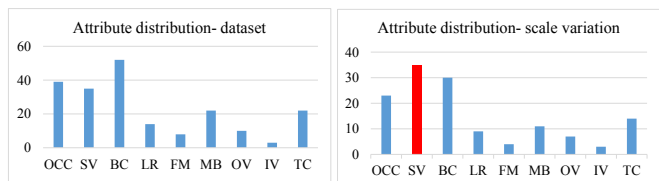


Fig. 2: The attributes distribution of the entire dataset and a scale variation subset.

B. Evaluation Methodology

There are two commonly used evaluation metrics in visual object tracking: center location error (CLE) and overlap ratio.

In this paper, we also adopt these two metrics to evaluate TIR pedestrian tracker. Follow to OTB [30], we use the precision and success rate for quantitative analysis.

Precision Plot. CLE is the average Euclidean distance between the tracked target and target’s ground-truth. If a CLE is within a given threshold (20 pixels), we say the tracking is successful in this frame. The precision plot measures the percentage of the successful frames in the entire dataset.

Success Plot. Overlap score measures the overlap ratio between the bounding box area of tracked target and ground-truth. If the score is larger than a given threshold, we say the tracking is successful in this frame. The success plot shows the ratios of successful frames at the threshold varying from 0 to 1. we use the area under curve (AUC) of each success plot to rank the trackers.

Robustness Evaluation. Usually, a tracker is sensitive to the initialization, and one-pass evaluation (OPE) does not provide the robustness evaluation. In order to measure a tracker’s robustness to the different initialization, we use the temporal robustness evaluation (TRE) and spatial robustness evaluation (SRE). TRE runs 20 times with different initial frame in a sequence, and then is to calculate the average precision and success rate. SRE runs 12 times with different initial bounding box by shifting or scaling.

Speed Evaluation. Speed is the other important aspect of a tracker. We run all trackers on the same hardware device and calculate their average frames per second (fps) in the entire dataset.

IV. EVALUATION EXPERIMENTS

In this section, we implement a large-scale fair evaluation experiments on the proposed benchmark. First, an overall performance evaluation of nine trackers is conducted in Section IV-A. Second, we evaluate the performance of these trackers on the attribute subset in Section IV-B. Third, a speed comparison experiment is presented in Section IV-C.

A. Overall Performance Evaluation

Evaluated Trackers. Nine public available trackers are evaluated on our benchmark. Since the TIR pedestrian trackers have no public available codes, we choose some commonly used visual trackers and TIR trackers for evaluation. These trackers can be used for the TIR pedestrian tracking and can be generally divided into four categories:

- Three correlation filter based trackers, kernelized correlation filters (KCF [31]), scale correlation filter (DSST [32]), spatially regularized correlation filters (SRDCF [33]).
- Two deep learning based trackers, HDT [34], MCFTS [35].
- Two regression based trackers, Ridge Regression (RR [13]), Gaussian regression (TGPR [36]).
- Two other trackers, SVM [13], sparse representation (LIAPG [37]).

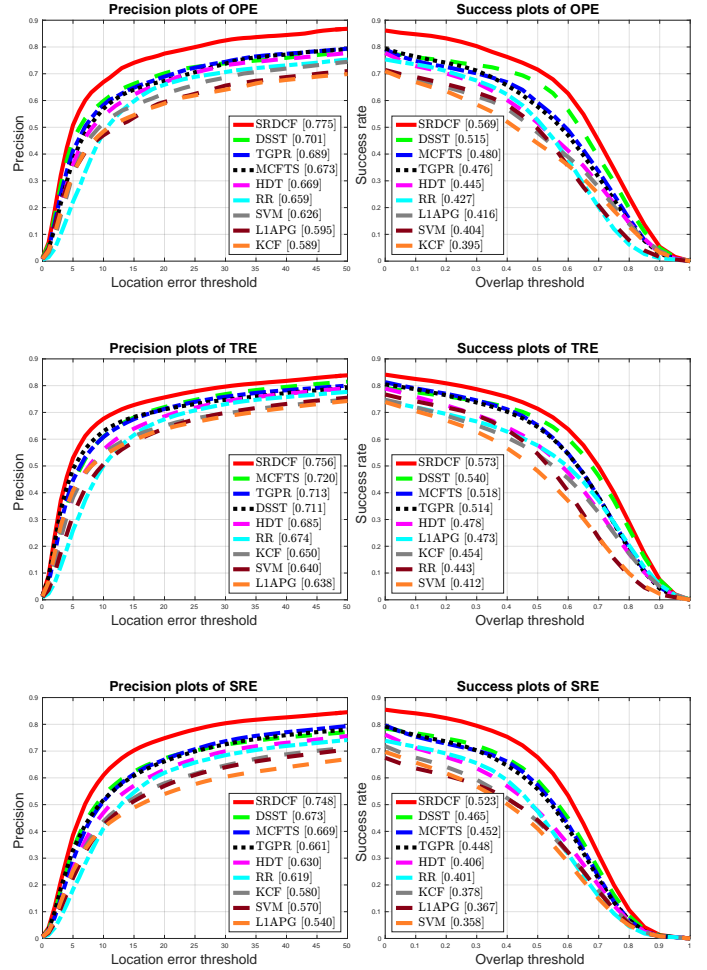


Fig. 3: The overall performance of the trackers using OPE, TRE, and SRE plots. The performance score is shown in the legend of the figures. The trackers are ranked in descending order according to their performance.

Most of these trackers have the state-of-the-art performance in visual tracking. For all of these trackers, we use the original parameters of them for evaluation.

Evaluation Results. Precision plots and success plots are used to show the overall performance of the tracker, and the results are shown in Fig. 3. OPE is used to show the precision and success rate of the tracker, while TRE and SRE are used to show the robustness of the tracker.

Analysis. The trackers are ranked according to their performance score. From Fig. 3, we can see that the ranking of the trackers are slightly different in the precision plots and success plots. This is because the evaluation metrics are different in these two plots. The precision is ranked according to the percentage of successful frames where center location error is within a fixed threshold (20 pixels), while the success rate is ranked according to AUC scores. We suggest that the success plots are more accurate than the precision plot for ranking.

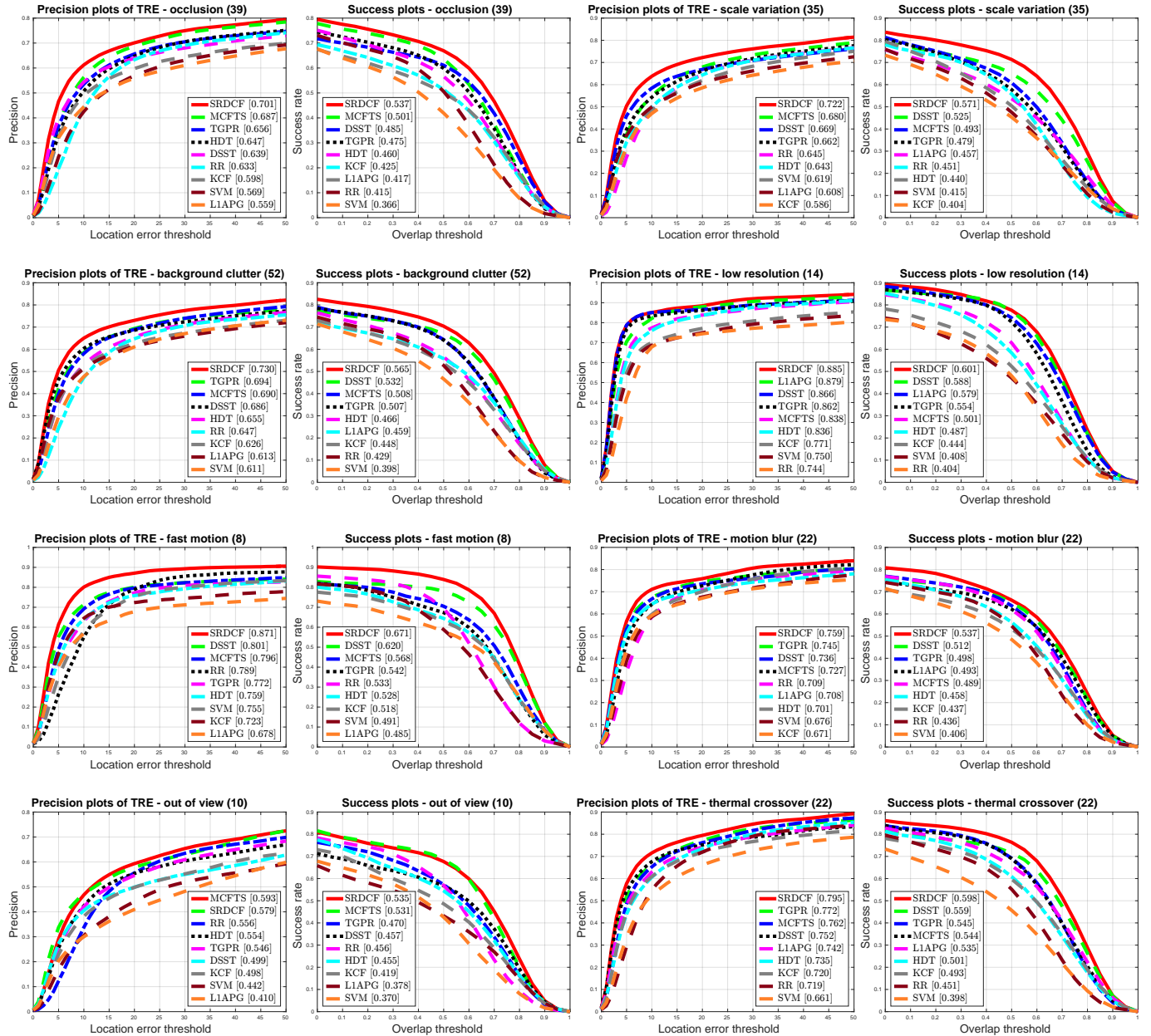


Fig. 4: TRE plots on eight attribute subsets. The title of the figure is the attribute name and corresponding sequences number.

Therefore, in the following, we mainly use the success plots to analyze the tracker’s ranking and use the precision plots as an auxiliary.

The tracker’s performance in TRE is higher than in OPE because the trackers tend to perform well in a shorter sequence. The OPE result is just one trial of TRE. On the contrary, the tracker’s performance in SRE is lower than in OPE since the initialization errors tend to cause the drift of the trackers.

In the success plots, we can see that SRDCF ranks the first one. That means its success rate and robustness are the best in all of these trackers. It is noteworthy that, SRDCF is much better than others. In the OPE and SRE, the performance of SRDCF is higher than the second best DSST more than 5%. In the TRE, it is also higher than DSST about 3%. We suggest that its superior performance benefits from the consideration of

more background information in tracking. On the other hand, it is easy to see that the performance of DSST is higher than KCF more than 10%. This shows that the scale estimation strategy is very important in the TIR pedestrian tracking.

Deep feature based TIR tracker MCFTS achieves a promising result despite the deep features are learned from the visible images. We suggest that the deep feature based trackers have potential to achieve better performance if there are enough thermal images for training. On the other hand, MCFTS just uses a simple combination method between the deep network and KCF. We consider a deeper level integration between of them can obtain more robust tracking results. In addition, we can see that the performance of Gaussian regression tracker TGPR is higher than ridge regression tracker RR about 5%. This is a prominent improvement. Therefore, we think a more

complexity kernel function is better than a simple one in the regression-based TIR pedestrian tracker.

B. Attribute-based Evaluation

Results. In order to understand the tracker’s performance for different challenges, we evaluate nine trackers on the attribute subsets, the results are shown in Fig. 4. Here, we just show the TRE plots on these subsets due to space limitation. OPE and SRE plots are presented in the **supplemental material**.

Analysis. The tracker’s performance on an attribute subset shows its ability to handle this challenge. As shown in Fig. 4, we can see that SRDCF achieves the best performance on almost all attribute subsets because it effectively solves the boundary effect brought from the cyclic shift. MCFTS achieves a better performance on the occlusion and out-of-view subset than DSST, despite DSST has the higher overall performance than MCFTS (see TRE of Fig. 3). That shows that the deep learning based trackers have a promising performance in the TIR pedestrian tracking. KCF and HDT have the worst performance on the scale variation subset since they lack the scale estimation strategy, while DSST obtains the second-best performance on the scale variation subset and the entire dataset since it deals with the scale variation. This demonstrates the scale estimation strategy is very useful to improve the tracking performance. On the fast motion subset, we can see that RR achieves a much higher success rate than its overall performance (see Fig. 3). We suggest that the stochastic particle filter search framework plays a major role. These results are helpful to us to understand the strength and weakness of the trackers.

C. Speed Comparison

We carry out the experiments on the same PC with an Intel I7-6700K CPU, 32G RAM, and a GeForce GTX 1080 GPU card. The speed of the tracker is the average fps on the TRE results. The comparison of the tracker’s speed is shown in Table IV.

Analysis. Table IV shows that KCF has a high speed while DSST also exceeds the real-time speed. The high efficiency of these two trackers benefits from the computation in the Fourier domain. What’s more, we can see SRDCF obtains a half of the real-time speed when it achieves the best precision and success rate. Two deep learning based trackers, HDT and MCFTS just get a low frame rate due to the high cost of the feature extraction. Several classifier based trackers such as SVM and RR also have a low speed because they base on a time-consuming particle filter search framework.

V. VALIDATION EXPERIMENTS

In this section, we conduct three comparison experiments to validate each component’s effectiveness to the TIR pedestrian tracking performance. First, we carry out a comparison experiment on a baseline tracker with six different features extractor in Section V-A. Then, a comparison experiment on a baseline tracker with three different motion models is implemented in

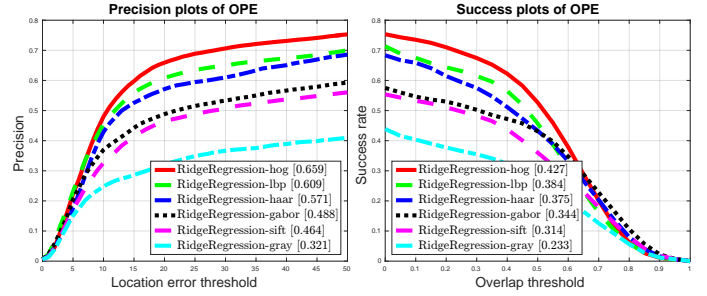


Fig. 5: OPE plots of the baseline tracker using six different feature extractors.

Section V-B. Finally, we compare several different observation models to validate how they affect the tracking performance in Section V-C.

A. Feature Extractor.

To understand the effect of the feature extractor to the TIR pedestrian tracking performance, we test six different features on a baseline tracker. These features are commonly used in the object detection and tracking.

- **Gray.** It simply resizes the image into a fixed size, and then uses the pixel values as features.
- **SIFT** [38]. It is a local feature descriptor and robust to the scale variation. Here, we use its fast version: dense SIFT using VLFeat toolkit [39].
- **Haar-like** [40]. It reflects the gray variation of the image. We use the simplest form, rectangular Haar-like features.
- **Gabor** [41]. It can capture the texture information of the image using a series of different direction’s Gabor filters.
- **LBP** [42]. It is a simple yet efficient local texture descriptor which has two advantages: rotation invariance and gray invariance.
- **HOG** [43]. It is used to capture the local gradient direction and gradient intensity distribution of the image.

We use Ridge Regression [13] as the baseline tracker, and the results are shown in Fig. 5.

Analysis. Fig. 5 shows that the baseline tracker using HOG feature achieves the best performance which is higher than the one using gray feature about 20%. It demonstrates that local gradient features are more helpful for TIR pedestrian tracking. Although the gray features are commonly used in the previous studies, it has a low discriminative ability for the TIR pedestrian object. The assumption that the object is warmer than its background is no longer suitable for TIR pedestrian tracking, because the TIR pedestrians often have similar intensity to their backgrounds. What’s more, we can see that the local texture feature LBP obtains second-best performance and it has a small gap to the best performance. This illustrates that along with the improvement of thermal image’s quality and resolution, texture features are useful for the TIR pedestrian tracking. Here, we not consider the deep

TABLE IV: Speed comparison of the trackers.

	KCF [31]	DSST [32]	SVM [13]	SRDCF [33]	HDT [34]	RR [13]	MCFTS [35]	L1APG [37]	TGPR [36]
FPS	393.40	96.30	13.40	12.29	10.60	6.64	4.73	3.66	1.77

feature extracted from the pre-trained network (e.g., VGG-Net [44]) since it is very slowly in this framework. It is not suitable for real-time tracking applications.

Findings. Feature extractor is the most important component in the TIR pedestrian tracker. It has a major effect to the TIR pedestrian tracker’s performance. Choosing or developing a strong feature can dramatically enhance the tracking performance.

B. Motion Model.

To understand the effect of the motion model to the TIR pedestrian tracking performance, we test three commonly used motion models on a baseline tracker with two different features.

- **Particle Filter** [45]. It is a sequential Bayesian importance sampling technique which belongs to the stochastic search method.
- **Sliding Window.** Sliding window is a kind of exhaustive search method. It simply considers all candidates within a square neighborhood.
- **Radius Sliding Window** [21]. Radius sliding window is an improvement version of the sliding window. It just considers all candidates within a circular region.

We also use Ridge Regression [13] as the baseline tracker, and the results are shown in Fig. 6.

Analysis. The particle filter has several advantages such as it can solve the scale variation problem, and recover from the tracking failure. However, from Fig. 6, it is easy to see that the particle filter is much worse than the sliding window when we use the weak feature (Gray) in the baseline tracker. We suggest that this is mainly because the gray feature lacks the discriminative power leading to the drift of the particle filter. On the contrary, when we use the strong feature (HOG) in the baseline tracker, three motion models perform the same good. It is interesting that the particle filter performs no any superiority to the tracking performance while it keeps a high computation complexity.

Findings. Different motion models have a minor effect to the tracker’s performance when the feature is strong enough. Therefore, a faster search strategy (e.g., sliding window) is more helpful for the TIR pedestrian tracking.

C. Observation Model.

Observation models are widely studied in the tracking field since the rapid development of the machine learning method. To understand the effect of the observation model to the TIR pedestrian tracking performance, we test four observation models using two different features.

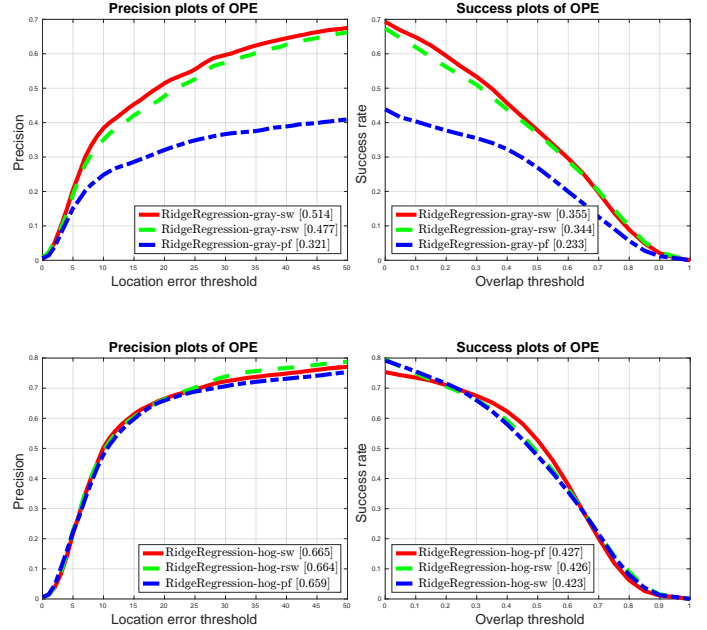


Fig. 6: OPE plots of the baseline tracker using three different motion models with two different feature extractors. The abbreviations pf, sw, rsw denotes the particle filter, sliding window, and radius sliding window respectively.

- **Logistic Regression.** It is a kind of linear regression with l_2 regularization. We use the gradient descent to update the model online.
- **Ridge Regression.** Least squares regression with l_2 regularization is used. The method comes from [13].
- **SVM.** It is a standard SVM with hinge loss and l_2 regularization.
- **Structured Output SVM (SOSVM).** This method is an enhanced version of SVM and comes from [21].

These four observation models are ranked according to their classification ability. The results are shown in Fig. 7.

Analysis. Fig. 7 shows that a strong observation model SOSVM achieves the best performance when the weak feature (Gray) is used. It exceeds the weak observation model Ridge Regression more than 10%. However, when we use the strong feature HOG, the weak observation model Ridge Regression obtains the best performance against the stronger SVM and SOSVM. What’s more, it is easy to see that these observation models have similar performance when the strong feature is used. Similar observations are reported in the visual tracking [13].

Findings. Strong observation model can obtain higher tracking performance when the feature is weakly. However, when the

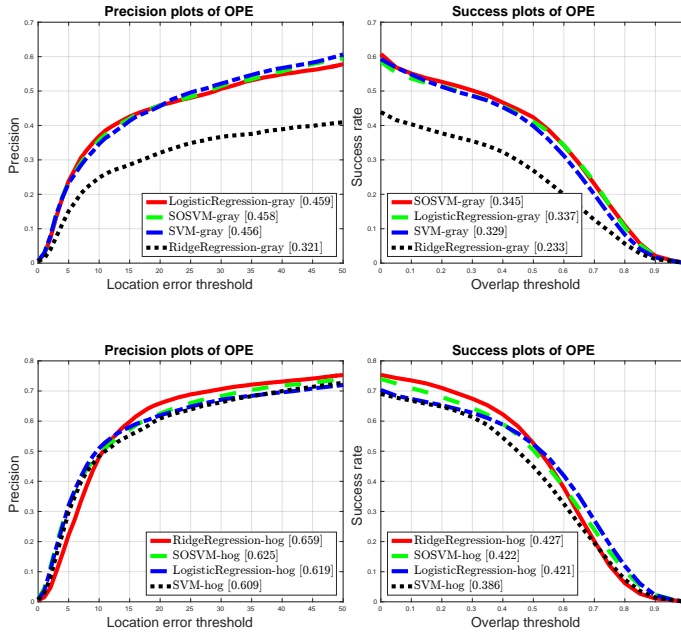


Fig. 7: OPE plots of the four tracker using different observation models with two different feature extractors.

feature is strong enough, different observation models have a minor gap in the tracking performance.

VI. CONCLUSION AND FUTURE WORK

In this paper, we collect a TIR pedestrian tracking benchmark dataset for the TIR pedestrian tracker evaluation. A large-scale evaluation experiment is carried out on our benchmark with nine public available trackers. Based on our evaluation results and analysis, several observations are highlighted for understanding the TIR pedestrian tracker. First, the scale estimation strategy is very important for TIR pedestrian tracking, and it can improve the tracking performance to a large extent. Second, the background information is crucial for a discriminative tracker, and it can enhance the discriminative power of the model. Third, deep learning based trackers have potential to obtain better performance in the TIR pedestrian tracking.

In addition, in order to understand the TIR pedestrian tracking more sufficiently, we conduct three validation experiments on each component of the tracker. Some interesting findings are helpful for the future research. First, the feature extractor is the most important component in the TIR pedestrian tracker, a strong feature can significantly improve the tracking performance. Second, different motion models have a minor effect on the tracking results when the feature is strong enough. Third, different observation models also have a minor effect on the tracking performance when the feature is strong. On the contrary, when the feature is weak, a stronger observation model often can achieve better performance.

The evaluation and validation experimental results help us to understand the TIR pedestrian tracker from several aspects.

This will promote the development of this field. In the future, we are going to extend the dataset to include more thermal sequences and explore more challenge factors in the TIR pedestrian tracking.

ACKNOWLEDGMENT

This research was supported by the National Natural Science Foundation of China (Grant Nos, 61272252, U1509216, 61472099, 61672183), by the Science and Technology Planning Project of Guangdong Province (Grant No. 2016B090918047), by the Natural Science Foundation of Guangdong Province (Grant No. 2015A030313544), and by the Shenzhen Research Council (Grant Nos. JCYJ20170413104556946, JCYJ20160406161948211, JCYJ20160226201453085, JSGG20150331152017052).

REFERENCES

- [1] R. Gade and T. B. Moeslund, "Thermal cameras and applications: a survey," *Machine vision and applications*, vol. 25, no. 1, pp. 245–262, 2014. **1**
- [2] J. Li and W. Gong, "Real time pedestrian tracking using thermal infrared imagery," *Journal of Computers*, vol. 5, no. 10, pp. 1606–1613, 2010. **1, 3**
- [3] J.-t. Wang, D.-b. Chen, H.-y. Chen, and J.-y. Yang, "On pedestrian detection and tracking in infrared videos," *Pattern Recognition Letters*, vol. 33, no. 6, pp. 775–785, 2012. **1, 3**
- [4] B. C. Ko, J.-Y. Kwak, and J.-Y. Nam, "Human tracking in thermal images using adaptive particle filters with online random forest learning," *Optical Engineering*, vol. 52, no. 11, pp. 113 105–113 105, 2013. **1, 2, 3, 4**
- [5] X. Li, R. Guo, and C. Chen, "Robust pedestrian tracking and recognition from flir video: A unified approach via sparse coding," *Sensors*, vol. 14, no. 6, pp. 11 245–11 259, 2014. **1, 2**
- [6] J. Portmann, S. Lynen, M. Chli, and R. Siegwart, "People detection and tracking from aerial thermal views," in *IEEE International Conference on Robotics and Automation (ICRA)*, 2014, pp. 1794–1800. **1**
- [7] Y. Ma, X. Wu, G. Yu, Y. Xu, and Y. Wang, "Pedestrian detection and tracking from low-resolution unmanned aerial vehicle thermal imagery," *Sensors*, vol. 16, no. 4, p. 446, 2016. **1**
- [8] T. Yang, D. Fu, and S. Pan, "Pedestrian tracking for infrared image sequence based on trajectory manifold of spatio-temporal slice," *Multimedia Tools and Applications*, vol. 76, no. 8, pp. 11 021–11 035, 2017. **1**
- [9] J. W. Davis and V. Sharma, "Background-subtraction using contour-based fusion of thermal and visible imagery," *Computer Vision and Image Understanding*, vol. 106, no. 2, pp. 162–182, 2007. **1, 2, 4**
- [10] R. Mieziako, "Ieee otcbs ws series benchmark," <http://vcip1-okstate.org/pbvs/bench/>, accessed March 4, 2018. **1, 2, 4**
- [11] J. Portmann, S. Lynen, M. Chli, and R. Siegwart, "People detection and tracking from aerial thermal views," in *IEEE International Conference on Robotics and Automation (ICRA)*, 2014, pp. 1794–1800. **1, 2, 4**
- [12] Z. Wu, N. Fuller, D. Thierault, and M. Betke, "A thermal infrared video benchmark for visual analysis," in *IEEE Conference on Computer Vision and Pattern Recognition (CVPR) Workshops*, 2014, pp. 201–208. **1, 2, 4**
- [13] N. Wang, J. Shi, D.-Y. Yeung, and J. Jia, "Understanding and diagnosing visual tracking systems," in *Proceedings of the IEEE International Conference on Computer Vision*, 2015, pp. 3101–3109. **1, 3, 5, 7, 8**
- [14] C. Dai, Y. Zheng, and X. Li, "Pedestrian detection and tracking in infrared imagery using shape and appearance," *Computer Vision and Image Understanding*, vol. 106, no. 2, pp. 288–299, 2007. **2**
- [15] K. Jüngling and M. Arens, "Pedestrian tracking in infrared from moving vehicles," in *IEEE Intelligent Vehicles Symposium*, 2010, pp. 470–477. **2, 3**
- [16] C. Liang, Q. Liu, and R. Xu, "Local sparse appearance model with specific structural information in infrared pedestrian tracking," in *IEEE International Conference on Image, Vision and Computing*, 2016, pp. 19–25. **2**
- [17] F. Xu, X. Liu, and K. Fujimura, "Pedestrian detection and tracking with night vision," *IEEE Transactions on Intelligent Transportation Systems*, vol. 6, no. 1, pp. 63–71, 2005. **2, 3, 4**

- [18] Z. Wang, Y. Wu, J. Wang, and H. Lu, "Target tracking in infrared image sequences using diverse adaboostsvm," in *International Conference on Innovative Computing, Information and Control*, 2006, pp. 233–236. [2](#), [4](#)
- [19] X. Wang and Z. Tang, "Modified particle filter-based infrared pedestrian tracking," *Infrared Physics & Technology*, vol. 53, no. 4, pp. 280–287, 2010. [2](#), [3](#)
- [20] D.-E. Kim and D.-S. Kwon, "Pedestrian detection and tracking in thermal images using shape features," in *International Conference on Ubiquitous Robots and Ambient Intelligence (URAI)*, 2015, pp. 22–25. [3](#)
- [21] S. Hare, S. Golodetz, A. Saffari, V. Vineet, M.-M. Cheng, S. L. Hicks, and P. H. Torr, "Struck: Structured output tracking with kernels," *IEEE transactions on pattern analysis and machine intelligence*, vol. 38, no. 10, pp. 2096–2109, 2016. [3](#), [8](#)
- [22] H. Grabner, M. Grabner, and H. Bischof, "Real-time tracking via on-line boosting," in *British Machine Vision Conference (BMVC)*, vol. 1, no. 5, 2006, p. 6. [4](#)
- [23] B. Babenko, M.-H. Yang, and S. Belongie, "Visual tracking with online multiple instance learning," in *IEEE Conference on Computer Vision and Pattern Recognition*, 2009, pp. 983–990. [4](#)
- [24] A. Torabi, G. Massé, and G.-A. Bilodeau, "An iterative integrated framework for thermal-visible image registration, sensor fusion, and people tracking for video surveillance applications," *Computer Vision and Image Understanding*, vol. 116, no. 2, pp. 210–221, 2012. [4](#)
- [25] Y. Socarrás, S. Ramos, D. Vázquez, A. M. López, and T. Gevers, "Adapting pedestrian detection from synthetic to far infrared images," in *International Conference on Computer Vision (ICCV) Workshop*, vol. 7, 2011. [4](#)
- [26] A. González, Z. Fang, Y. Socarras *et al.*, "Pedestrian detection at day/night time with visible and fir cameras: A comparison," *Sensors*, vol. 16, no. 6, p. 820, 2016. [4](#)
- [27] M. Felsberg, M. Kristan, J. Matas, A. Leonardis *et al.*, *The Thermal Infrared Visual Object Tracking VOT-TIR2016 Challenge Results*, 2016, pp. 824–849. [4](#)
- [28] INO, "Ino video analytics dataset," www.ino.ca/en/video-analytics-dataset/, accessed March 4, 2018. [4](#)
- [29] Youtube, "Youtube thermal videos," www.youtube.com, accessed March 4, 2018. [4](#)
- [30] Y. Wu, J. Lim, and M.-H. Yang, "Online object tracking: A benchmark," in *IEEE Conference on Computer Vision and Pattern Recognition (CVPR)*, 2013, pp. 2411–2418. [5](#)
- [31] J. F. Henriques, R. Caseiro, P. Martins, and J. Batista, "High-speed tracking with kernelized correlation filters," *IEEE Transactions on Pattern Analysis and Machine Intelligence*, vol. 37, no. 3, pp. 583–596, 2015. [5](#), [8](#)
- [32] M. Danelljan, G. Häger, F. Khan, and M. Felsberg, "Accurate scale estimation for robust visual tracking," in *British Machine Vision Conference (BMVC)*, 2014. [5](#), [8](#)
- [33] M. Danelljan, G. Hager, F. Shahbaz Khan, and M. Felsberg, "Learning spatially regularized correlation filters for visual tracking," in *IEEE International Conference on Computer Vision (ICCV)*, 2015, pp. 4310–4318. [5](#), [8](#)
- [34] Y. Qi, S. Zhang, L. Qin, H. Yao, Q. Huang, J. Lim, and M.-H. Yang, "Hedged deep tracking," in *IEEE Conference on Computer Vision and Pattern Recognition (CVPR)*, 2016, pp. 4303–4311. [5](#), [8](#)
- [35] Q. Liu, X. Lu, Z. He, C. Zhang, and W.-S. Chen, "Deep convolutional neural networks for thermal infrared object tracking," *Knowledge-Based Systems*, vol. 134, pp. 189–198, 2017. [5](#), [8](#)
- [36] J. Gao, H. Ling, W. Hu, and J. Xing, "Transfer learning based visual tracking with gaussian processes regression," in *European Conference on Computer Vision (ECCV)*, 2014, pp. 188–203. [5](#), [8](#)
- [37] C. Bao, Y. Wu, H. Ling, and H. Ji, "Real time robust l1 tracker using accelerated proximal gradient approach," in *IEEE Conference on Computer Vision and Pattern Recognition (CVPR)*, 2012, pp. 1830–1837. [5](#), [8](#)
- [38] D. G. Lowe, "Object recognition from local scale-invariant features," in *IEEE International Conference on Computer Vision (ICCV)*, 1999, pp. 1150–1157. [7](#)
- [39] A. Vedaldi and B. Fulkerson, "VLFeat: An open and portable library of computer vision algorithms," <http://www.vlfeat.org/>, 2008. [7](#)
- [40] P. Viola and M. Jones, "Rapid object detection using a boosted cascade of simple features," in *IEEE Conference on Computer Vision and Pattern Recognition (CVPR)*, vol. 1, 2001, pp. I–I. [7](#)
- [41] M. Haghghat, S. Zonouz, and M. Abdel-Mottaleb, "Cloudid: Trustworthy cloud-based and cross-enterprise biometric identification," *Expert Systems with Applications*, vol. 42, no. 21, pp. 7905–7916, 2015. [7](#)
- [42] T. Ojala, M. Pietikainen, and D. Harwood, "Performance evaluation of texture measures with classification based on kullback discrimination of distributions," in *IEEE International Conference on Pattern Recognition (ICPR)*, vol. 1, 1994, pp. 582–585. [7](#)
- [43] N. Dalal and B. Triggs, "Histograms of oriented gradients for human detection," in *IEEE Conference on Computer Vision and Pattern Recognition (CVPR)*, vol. 1, 2005, pp. 886–893. [7](#)
- [44] K. Simonyan and A. Zisserman, "Very deep convolutional networks for large-scale image recognition," *arXiv preprint arXiv:1409.1556*, 2014. [8](#)
- [45] B. Ristic, S. Arulampalam, and N. J. Gordon, *Beyond the Kalman filter: Particle filters for tracking applications*. Artech house, 2004. [8](#)